Oxidation of 2,5-diformfylfuran to 2,5-furandicarboxylic acid catalyzed by Candida antarctica Lipase B immobilized in a cyclodextrin-templated mesoporous silica. The critical role of pore characteristics on the catalytic performance

Cédric Decarpigny, Rudina Bleta, Anne Ponchel, Eric Monflier

Oxidation of 2,5-Diformylfuran to 2,5-Furandicarboxylic Acid Catalyzed by *Candida antarctica* Lipase B Immobilized in a Cyclodextrin-Templated Mesoporous Silica. The Critical Role of Pore Characteristics on the Catalytic Performance

Cédric Decarpigny,[1] *Rudina Bleta,*[*1] *Anne Ponchel,*[1] *Eric Monflier*[1]

[1]Univ. Artois, CNRS, Centrale Lille, ENSCL, Univ. Lille, UMR 8181-UCCS-Unité de Catalyse et Chimie du Solide, F-62300 Lens, France.

***Corresponding Author: E-mail:** rudina.bleta@univ-artois.fr

Abstract

Hypothesis: Porous silica has been extensively used as suitable carrier for the immobilization of various enzymes. Randomly Methylated β-Cyclodextrin (RaMeβCD) has surface active properties and very high solubility in water and could therefore be used as template in the fabrication of silica particles with tunable pore size.

Experiments: Silica particles were prepared by sol-gel process in alkaline medium with and without use of RaMeβCD. Lipase B from *Candida antarctica* (CALB) was either incorporated

within the pores of RaMeβCD-derived support or covalently attached on the surface of CD-free silica particles and its catalytic performance was assayed in the oxidation of 2,5-diformylfuran (DFF) to 2,5-furandicarboxylic acid (FDCA). Enzymatic reactors were characterized by N_2-adsorption analysis, small angle XRD, TG/DSC experiments, ATR-FTIR spectroscopy, HR-TEM and LSCM, while reaction products were determined based on ^{1}H NMR spectroscopy combined with HPLC.

Findings: Results showed that the use of RaMeβCD as structure directing agent led to mesoporous silica composed of uniform 8 nm-sized particles with 11 nm-sized mesopores compatible with the dimensions of CALB (3.0 nm x4.0 nm x5.0 nm). Incorporation of CALB within the pores of RaMeβCD-derived silica caused almost a two-fold increase in specific activity after 7 hours at 40 °C when compared to lipase immobilized on the surface of CD-free silica particles (33.2 μmol g^{-1} min^{-1} *vs.* 14.4 μmol g^{-1} min^{-1}). Moreover, the RaMeβCD-derived biocatalyst demonstrated enhanced operational stability during the recycling experiments, retaining more than 90% of its initial activity after five 24 h-reaction cycles. These findings open up new avenues for future research on the use of cyclodextrins in the development of enzyme-based nanoreactors.

Keywords: cyclodextrin, mesoporous silica, Stöber process, enzyme, biocatalysis, 2-diformyfuran, 2,5-furandicarboxylic acid.

1. Introduction

Enzymes are versatile biocatalysts produced by living cells and also rightly called the catalytic machinery of living systems as they are responsible for catalyzing a multitude of chemical

reactions in a variety of biological processes [1, 2]. For several decades, enzymes from microorganisms have occupied an important place in a range of industrial relevant processes such as wine fermentation [3, 4], cheese manufacture [5], glucose production from starch [6], as well as detergent and textile industries [7]. Over the past few decades, the rapid progress in enzyme engineering has strongly encouraged chemical industries to embrace enzyme technology [8], a trend supported by the current environmental issues [9] and the sustainable development goals [10, 11].

One of the major concerns in industrial application of enzymes is their limited operational stability with regard to reaction conditions, their high cost, as well as the difficulty in recovering and reusing the biocatalyst [12]. To overcome some of these limitations and make a balance between cost and benefits of enzyme applications, immobilization procedures in a solid support can be used [12, 13, 14, 15]. Several immobilization strategies have been proposed in literature, including the multipoint covalent attachment to increase enzyme rigidity [16], the multisubunit immobilization to reduce subunit dissociation [17], the introduction of suitable functional groups to create a favorable surrounding microenvironment [18], or the confinement into the pores of the carrier to minimize protein aggregation [19]. Nevertheless, in some cases, immobilization may also cause deactivation of the biocatalyst due to conformational changes of the surface bound enzyme with respect to its native state [20]. In this sense, the design of supporting materials with adequate pore architecture that can provide sufficient free space to preserve conformational freedom of the protein and avoid blocking of the active site, while reducing enzyme leakage, is of fundamental importance for an efficient immobilization strategy.

Porous materials prepared by template-directed approaches have emerged as promising carriers for the immobilization of enzymes [21, 22, 23]. As demonstrated by several studies, pores not

only improve the biochemical stability of the enzyme [24], but they also have a relevant importance in the diffusion of reactants and products during the catalytic process [25]. Among the solid carriers, mesoporous silica has attracted much interest owing to its high thermal and pH stability, functionalizable surface, as well as ease of preparation [21]. Soft-template methods using block copolymers with different geometries and block lengths as template, in combination or not with swelling agents (e.g., alkyl-substituted benzenes) [26, 27], as well as the supramolecular assemblies formed between nonionic polymers and native cyclodextrins in water [36] have been shown to be particularly effective in a fine tuning of the pore size of silica.

Cyclodextrins (CDs) are water-soluble cyclic oligosaccharides with a toroidal shape composed of α-(1,4)-linked glucopyranose subunits. They possess an exterior hydrophilic surface covered by primary and secondary hydroxyl groups and an internal hydrophobic cavity containing CH_2 groups, which make them particularly attractive for construction of supramolecular architectures through host-guest interactions [28, 29]. The most common CDs are alpha-, beta- and gamma-CDs having respectively six, seven and eight glucopyranose subunits in the ring and among them, β-CD has received the greatest attention due to its high binding affinity and cost effectiveness [28, 29]. Randomly methylated β-CD (RaMeβCD) is one of the most widely used β-CD derivatives with a degree of substitution of 12.6 and a particular molecular structure conferring to this CD surface-active properties and very high solubility in water (>500 mg/mL) (Figure S1, ESI).

Over the last two decades, CD-containing polymers and dendrimers, as well as metallic and metal oxide surfaces capped with terminal CD moieties have been widely utilized as supports for the supramolecular attachment of proteins by host-guest interactions [30, 31, 32]. In materials science, CDs have also been explored for the synthesis of silica nanostructures with various pore

architectures [33, 34, 35], but the practical applications of those materials are still limited. Our group has recently shown that these oligosaccharides may be employed efficiently as soft templates to direct the synthesis of hierarchically structured porous silica [36] and mesoporous metal oxides [37, 38] with enhanced activity in photocatalysis [39], heterogeneous catalysis [40, 41] and biocatalysis [42].

Here, we report a simple and efficient RaMeβCD-modified Stöber approach for the fabrication in aqueous phase of mesoporous silica with tunable pore size and demonstrate its use as an efficient carrier for the immobilization of lipase B from *Candida antarctica* (CALB). Lipases (triacylglycerol acylhydrolases EC 3.1.1.3) are versatile biocatalysts catalyzing hydrolysis, esterification and transesterification reactions and are widely used in food, pharmaceutical, detergent and chemical industries [43]. The catalytic activity of lipases is greatly enhanced at lipid/water interfaces by a phenomenon known as "interfacial activation". Hence, the active site of lipases is naturally covered by a polypeptide chain called "lid" and in the presence of a lipid/water interface, the lid opens exposing a large hydrophobic surface of the active site to the substrate. CALB is probably one of the most important lipases currently used in many industrial applications owing to its high selectivity towards secondary alcohols and secondary amines [44, 45], as well as its high resistance towards hydrogen peroxide [46, 47]. In this study, we evaluate the activity of immobilized CALB in the oxidation of 2,5-diformylfuran (DFF) to 2,5-furandicarboxylic acid (FDCA), which is listed as one of the 12+2 most important biomass-derived platform chemicals. FDCA has also been identified as a highly promising substituent for the terephtalic acid, the precursor of polyethylene terephthalate (PET) used in the production of plastic bottles, films and fibers [48, 49]. The oxidation of DFF to FDCA proceeds *via* a chemoenzymatic cascade reaction involving two consecutive reaction steps [42, 50]. First, the

lipase CALB catalyzes the reversible formation of peracetic acid from ethyl acetate and hydrogen peroxide. Then, the peracid generated *in-situ* oxidizes the aldehyde group of DFF to carboxylic acid yielding the 5-formylfuran-2-carboxylic acid (FFCA), which is ultimately converted to FDCA (Scheme 1). We show for the first time that CALB incorporated into the pores of a RaMeβCD-templated mesoporous silica prepared by a modified Stöber process may present enhanced catalytic activity and stability with respect to the lipase immobilized on the surface of CD-free silica particles.

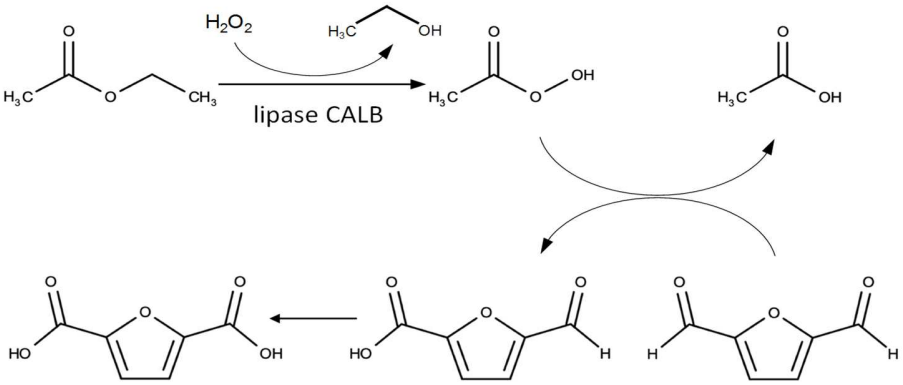

Scheme 1. Chemo-enzymatic selective oxidation of DFF to FDCA.

2. Results and discussion

2.1 Method for the preparation of the supported biocatalysts

Two types of silica particles with different sizes and pore diameters were prepared and further utilized as supports for the immobilization of CALB (Figure 1). In a first synthesis, bimodal sized particles with 6 nm and 75 nm mean diameters and two sets of pores (3.4 nm and 33 nm diameters) were prepared by conventional Stöber process in an alkaline medium using tetraethyl orthosilicate (TEOS) as silica source. In a second synthesis, RaMeβCD was employed as structure directing agent yielding 8 nm-sized particles with uniform 11.2 nm-sized pore

diameters and almost twice higher pore volume. DLS results revealed formation of large aggregates of RaMeβCD with 106 nm hydrodynamic radius (R_H) coexisting with non-associated oligosaccharides (R_H = 0.95 nm) (Figure S5, ESI). On the other hand, the surface tension measurements indicated a decrease in the surface tension of water from 72 mN/m to 58.4 mN/m at 20 mM RaMeβCD reflecting the surface-active properties of this cyclodextrin which would be beneficial for the self-assembly of silica particles (Figure S6, ESI).

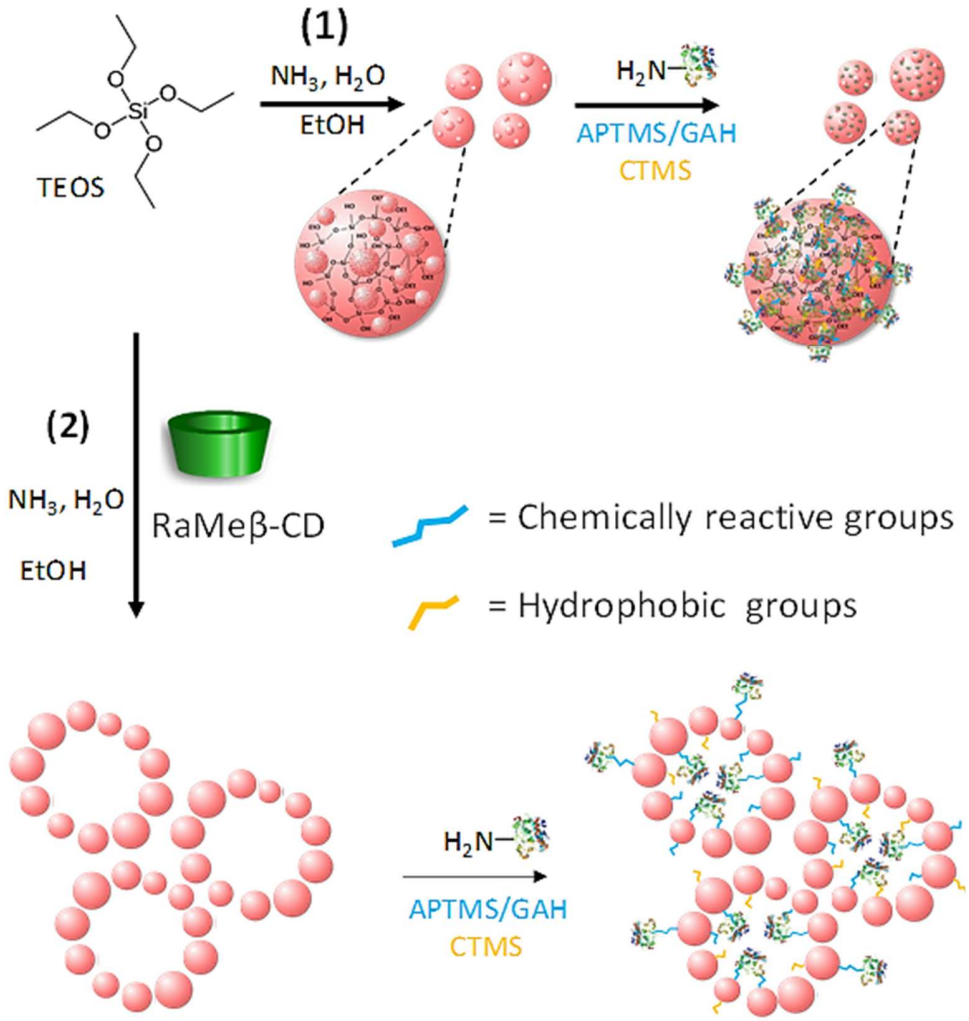

Figure 1. Schematic illustration of the immobilization of CALB on silica particles prepared by conventional (1) and RaMeβCD-modified (2) Stöber method. Prior to lipase immobilization, supports were functionalized with hydrophobic trimethyl groups derived from

chlorotrimethylsilane (CTMS) and chemically reactive groups derived from the 3-aminopropyltrimethoxysilane (APTMS), activated with glutaraldehyde (GAH).

In both syntheses, silica surface was further modified with glutaraldehyde (GAH)-activated amine groups derived from the 3-aminopropyltrimethoxysilane (APTMS) used for the covalent anchoring of the lipase, as well as hydrophobic trimethyl groups derived from the chlorotrimethylsilane (CTMS), necessary for its interfacial activation. Based on the study of Monsan[51] who has proposed a glutaraldehyde reaction mechanism involving two molecules of GAH per amino group in Spherosil silica at pH 7, the amount of GAH used in our study was in excess to that required for activation (GAH/APTMS molar ratio = 6.7). The excess of GAH was then washed off before enzyme coupling. The catalytic performance of the immobilized lipase was then evaluated in the oxidation of 2,5-diformylfuran (DFF) to 2,5-furandicarboxylic acid (FDCA) and was correlated to the pore characteristics of the supports.

2.2 Characterization of the supports.

TG-DSC analysis in flowing air were performed to estimate the amount of cyclodextrin incorporated within the silica matrix (Figure S7, ESI). To minimize the effect of solvent adsorbed into the pores, the weight loss below 180 °C was not taken into consideration.

In the temperature range between 180 and 700 °C, the template-free sol-gel SiO_2 (Figure S7 A, ESI) displayed a total weight loss of 6.5 wt.% corresponding mainly to polycondensation and dehydration reactions [52]. The exothermic peak at 360 °C assigned to the oxidation of the ethoxy groups [53] indicates that TEOS is not completely hydrolyzed and residual $-OCH_2CH_3$ groups still remain on the particle surface. In comparison, the RaMeβCD-templated material (Figure S7 B, ESI) displayed an additional exothermic peak at 470 °C, which may be assigned to

the decomposition of the oligosaccharide. The weight loss recorded in the temperature range of 180-700°C was 8.7 % and the remaining amount of cyclodextrin, calculated by the difference between the mass loss of RaMeβCD-SiO_2 minus the mass loss of SiO_2, was estimated to be 2.2%.

The adsorption isotherms and corresponding pore size distributions of SiO_2 and RaMeβCD-SiO_2 materials are depicted in Figure 2. Both isotherms present an hysteresis loop once a threshold relative pressure is reached, highlighting the presence of mesopores (Figure 2 A). At low relative pressures ($P/P_0 < 0.4$), the amount of nitrogen adsorbed is almost identical in both materials indicating similar surface areas; however at higher relative pressures ($P/P_0 > 0.4$), the rapid increase of the N_2 uptake recorded on RaMeβCD-SiO_2 solid points out an enhancement of the pore volume. Indeed, the BET surface areas (S_{BET}) were measured to be 450 and 432 m^2/g for SiO_2 and RaMeβCD-SiO_2 respectively, whereas the total pore volume (V_p) was almost doubled, from 0.487 to 0.969 cm^3/g, when RaMeβCD was used as structure directing agent (Table 1).

The pore size distribution curves determined from the BJH method further illustrate the contrasting pore characteristics of these two solids (Figure 2 B). Indeed, the SiO_2 material showed a broader and less well-defined pore size distribution with two types of mesopores of approximately 3.4 nm and 33 nm diameters (Figure 2 B inset). Macropores were also present, as revealed by the continuous increase of the adsorbed volume at high relative pressures ($P/P_0 \approx 1$).

In a quite different way, the material prepared from RaMeβCD exhibited a sharper pore condensation step, indicative of pores with uniform diameters. Accordingly, the pore size distributions of RaMeβCD-SiO_2 were unimodal with an average pore diameter of 11.2 nm, occupying a much larger pore volume with respect to SiO_2. The micropore volumes obtained

from the t-plot represented 6.2% and 1.8% of the total pore volume of SiO_2 and RaMeβCD-SiO_2 respectively (Table 1).

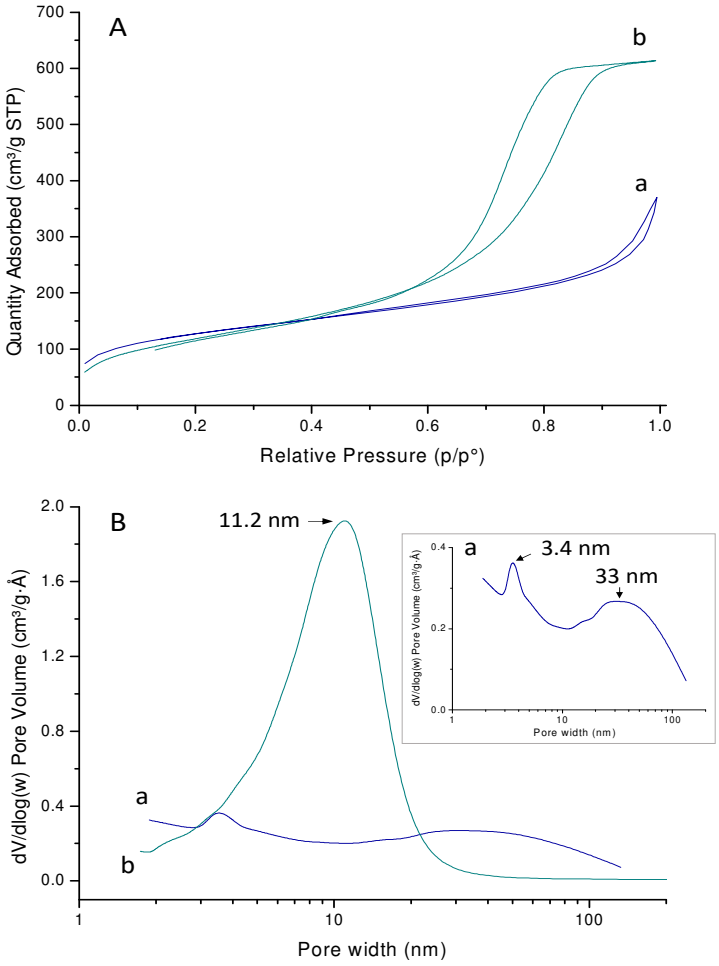

Figure 2. N_2-adsorption isotherms (A) and corresponding pore size distributions (B) of SiO_2 (a) and RaMeβCD-SiO_2 (b) materials.

TEM images revealed that the SiO_2 material was composed of round-shape particles with an average diameter of 75 nm decorated on their surface with small-sized particles of approximately 6 nm diameter (Figure 3 A). Mesopores were build-up by primary particles, while macropores resulted from the packing of primary particles in agglomerates. Conversely, the RaMeβCD-SiO_2

material consisted mainly of small-sized particles with uniform 8 nm diameter assembled in a sponge-like porous network (Figure 3 B). The white areas in the TEM micrographs are representative of mesopores originating from the interstitial spaces between primary particles.

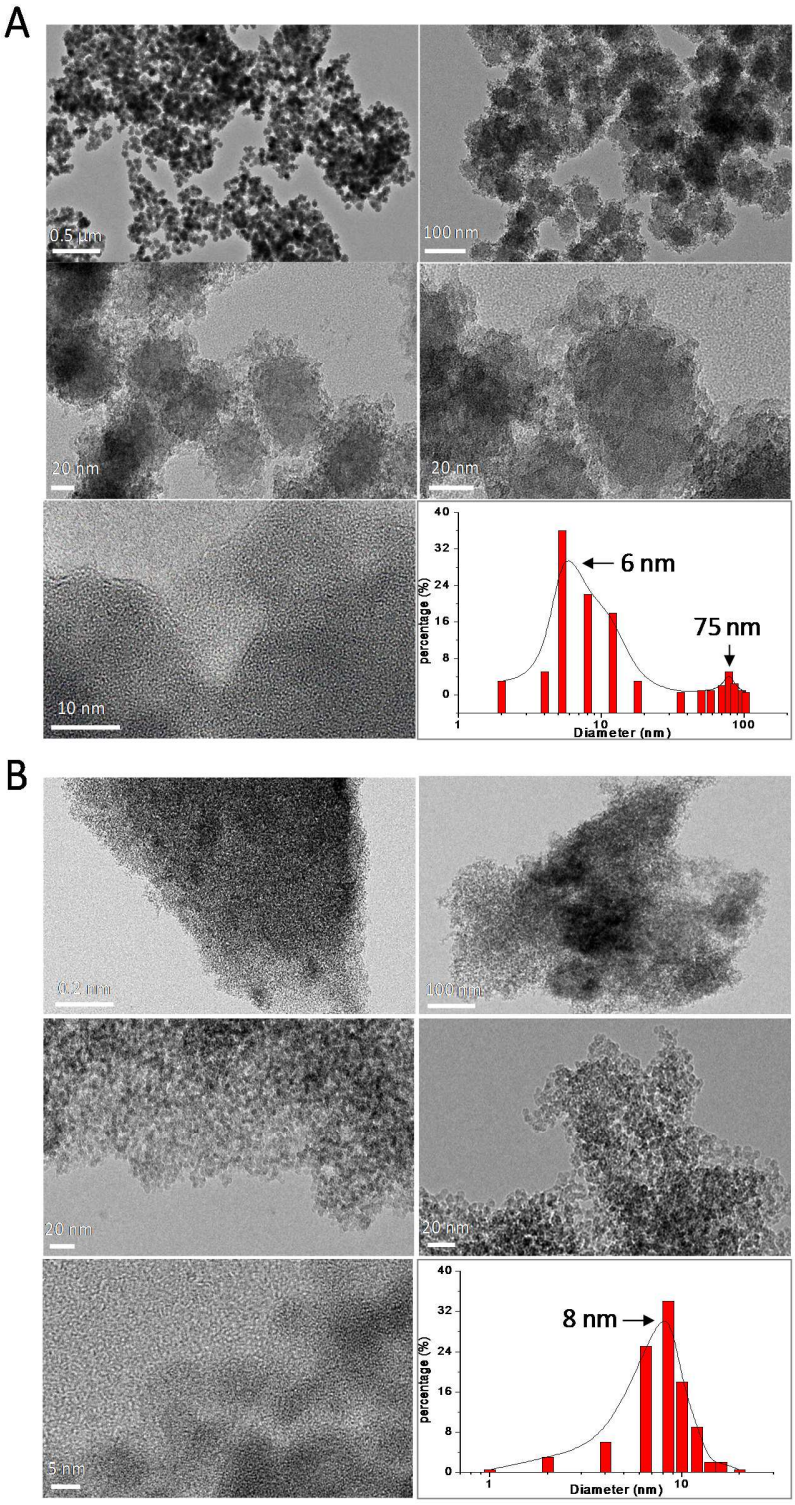

Figure 3. TEM images and corresponding particle size distribution of SiO_2 (A) and RaMeβCD-SiO_2 (B) materials.

From the small angle X-ray scattering diagrams (Figure S8, ESI), it can be seen that the RaMeβCD-SiO_2 solid displayed a well-defined correlation peak at 2Θ = 1.62° corresponding to a d-spacing of 2.7 nm ($d_{Bragg} = n\lambda/2\sin\theta$). This means that some local organization of the mesopores exists within the silica network although the absence of high order peaks suggests a lack of overall long-range ordering. Moreover, the shift of the diagram of RaMeβCD-SiO_2 to higher 2Θ values with respect to SiO_2 is consistent with a decrease in the interparticular separation, in agreement with TEM observations.

Taken together, these characterization results confirm that RaMeβCD plays an important role in improving both the structural and textural characteristics of the silica particles, which in turn can affect the activity and stability of the enzyme.

2.3 Silanization of the support and enzyme immobilization. Prior to lipase grafting, the as-synthesized silica particles were modified with hydrophobic trimethyl groups derived from the chlorotrimethylsilane (CTMS) and chemically reactive amine groups derived from the 3-aminopropyltrimethoxysilane (APTMS). Functionalization with APTES was followed by activation of aminated silica support with a bifunctional spacer, *i.e.* the glutaraldehyde (GAH), which provides an aldehyde group that reacts with the amino groups of lysine residues, resulting in the formation of an imine bond (Schiff base). To identify the different functional groups anchored on the silica surface, attenuated total reflectance Fourier transform infrared spectroscopy (ATR-FTIR) and thermogravimetric (TG) analyses were carried out.

ATR-FTIR spectra of non-functionalized SiO_2 and RaMeβCD-SiO_2 (Figure 4 A-a, B-a) displayed two intense bands at 1061 and 800 cm^{-1} ascribed to the asymmetric and the symmetric stretching vibrations respectively of the Si-O-Si bond [54]. Upon surface modification, the attenuation of the vibration band at 959 cm^{-1} arising from the symmetric stretching of the Si-OH

groups confirmed successful functionalization of surface silanols. Indeed, the strong vibration bands at 1566 cm^{-1} and 1417 cm^{-1} are consistent with the N-H bending of the primary amine and the symmetric CH_2 bending of Si-CH_2 groups respectively ((Figure 4 A-b, B-b). Furthermore, the Si-C stretching vibration at 856 cm^{-1} from the -O-$SiCH_3$ end groups is indicative of effective surface functionalization with trimethylsilyl groups. The covalent anchoring of the enzyme on SiO_2@CAG and RaMeβCD-SiO_2@CAG supports was confirmed by the vibration band at 1640 cm^{-1} characteristic of the imine bond (C=N) resulting from the interaction between the aldehyde groups of the glutaraldehyde and the primary amine groups of the lysine ((Figure 4 A-c, B-c). Moreover, the increase in the intensity of the vibration at 1566 cm^{-1} corresponding to the N-H bending of free amines is another indication of successful protein grafting. It is worth noting that as the immobilization of lipase was carried out at pH 4.6, that is in the interval between the isoelectric point of CALB (pI = 6.0) and the point of zero charge of silica (PZC = 2.0), ionic binding and hydrophobic interactions are also likely to occur, therefore facilitating the rapprochement of lipase to the activated support before its covalent attachment.

The amount of functional groups anchored on the silica surface was estimated from the thermogravimetric analysis by the difference between the mass loss of the functionalized matrix minus the mass loss of the bare matrix in the temperature range between 180 °C and 700 °C (Figure S9 ESI). The loadings of surface functional groups measured on SiO_2@CAG (Figure S9 A,b ESI) and RaMeβCD-SiO_2@CAG (Figure S9 B,b ESI) were almost equal, *i.e.* 22.3 wt% and 22.2 wt% respectively, because both supports have nearly the same surface area, *i.e.* 450 m^2/g and 432 m^2/g respectively (Table 1). Nevertheless, RaMeβCD-SiO_2 solid exhibited a higher grafting density of trimethyl groups compared to SiO_2 (60 mg/g *vs.* 38 mg/g), but presented a

lower weight loss in the temperature range of 40-180°C (26 mg/g *vs.* 57 mg/g) consistent with its higher degree of hydrophobicity (Figure S10, Table S1, ESI).

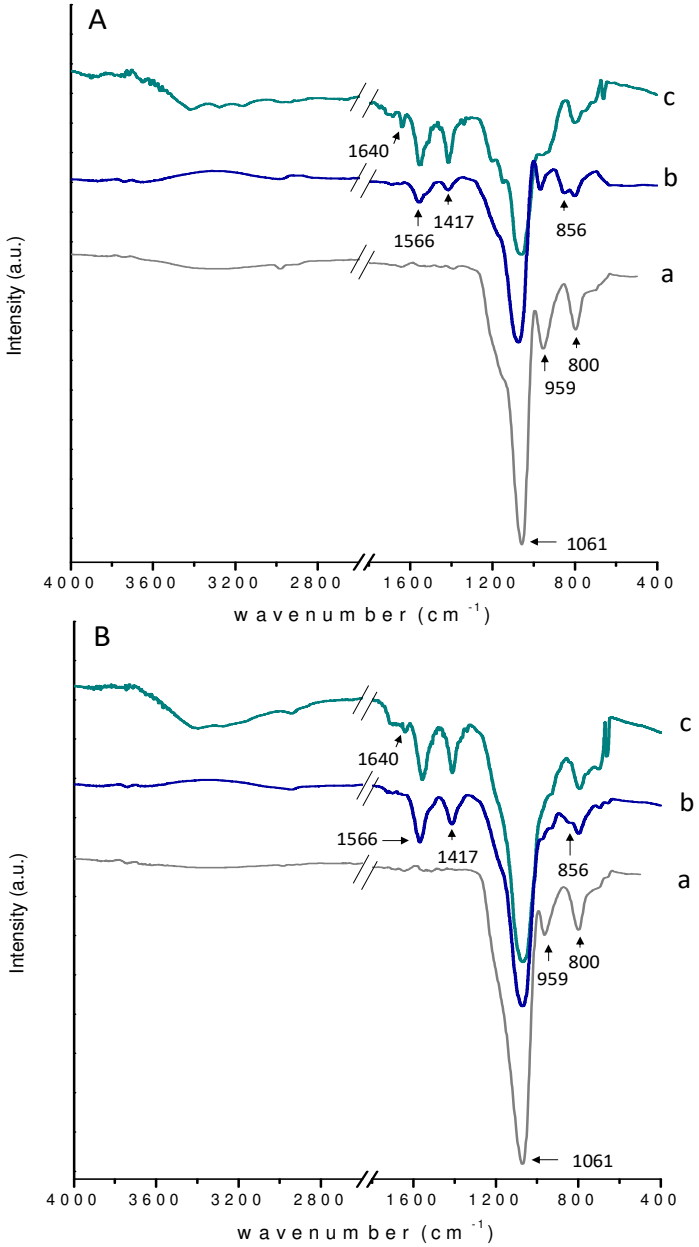

Figure 4. ATR-FTIR spectra of silica supports prepared without (A) and with RaMeβCD (B): (a) non-functionalized support; (b) support@CAG; (c) support@CAG@CALB.

Using equation 1 (ESI), the corresponding surface coverages (S_{cov}) were determined to be 0.66 chain/nm^2 and 1.02 chain/nm^2 for SiO_2@C and RaMeβCD-SiO_2@C respectively. Considering that organosilanes form a monolayer on the silica surface and that each trimethyl ligand occupies a surface of 0.43 nm^2, the maximum grafting densities (D_g^{max}) for SiO_2@C and RaMeβCD-SiO_2@C were determined to be 189 mg/g and 181 mg/g respectively (equation 2, ESI). As can be noted, the grafting densities determined from TG analysis are much lower than those estimated from the surface areas, suggesting that the surface of silica particles can be only partially covered by the hydrophobic trimethyl groups.

Table 1. Parameters deduced from N_2-adsorption and TG analysis for the silica materials before and after modification with different functional groups and lipase immobilization.

Sample	N_2-adsorption				TG analysis	
	S_{BET}[a] ($m^2.g^{-1}$)	V_p[b] ($cm^3.g^{-1}$)	D_p[c] (nm)	% µpore[d]	total weight loss (%)[e]	effective weight loss (w%)[f]
SiO_2	450	0.487	3.4 and 33	6.2	6.5	-
RaMeβCD-SiO_2	432	0.969	11.2	1.8	8.7	2.2
SiO_2@CAG	39	0.178	39	0.2	28.8	22.3
RaMeβCD-SiO_2@CAG	278	0.628	8.1	4.8	30.9	22.2
SiO_2@CAG@CALB	17	0.246	45	0.3	35.5	6.7
RaMeβCD-SiO_2@CAG@CALB	212	0.474	6.5	4.1	38.3	7.4

[a]BET specific surface area determined in the relative pressure range 0.1-0.25, [b]cumulative pore volume (BJH), [c]pore diameter calculated from BJH method, [d]% micropores = (V_{micro}/V_P)*100 where V_{micro} is the micropore volume determined from the t-plot, [e]weight loss between 180 and 700 °C, [f]weight loss corrected by the decomposition profile of sol-gel silica before surface functionalization.

Despite their different pore characteristics, these two materials presented were very similar enzyme loading capacities *i.e.* 6.4 wt.% for SiO_2 and 7.4 wt.% for RaMeβCD-SiO_2 (Figure S9

ESI, Table 1). However, notable differences were evidenced on the location of the protein, which was found either to bind on the surface of SiO_2@CAG particles or to be incorporated within the pore structure of RaMeβCD-SiO_2@CAG. Indeed, as revealed by N_2-adsorption analysis (Figure 5), the surface area of SiO_2 decreased drastically from 450 m^2/g to 39 m^2/g upon grafting of trimethyl and aminopropyl groups and further activation with glutaraldehyde. Similarly, the pore volume was also reduced by almost one-third (from 0.487 to 0.178 cm^3/g) (Table 1), while the smallest pores at 3.4 nm totally disappeared.

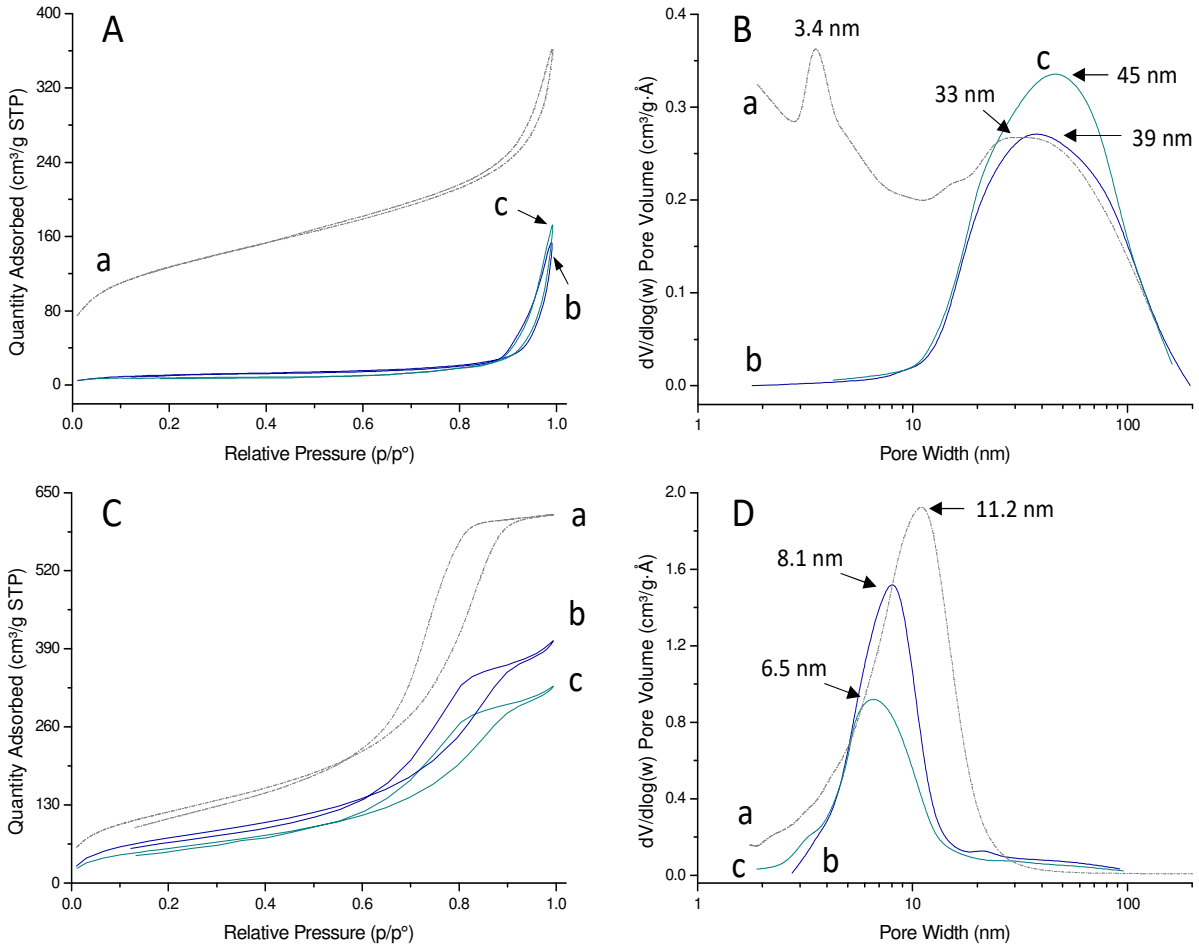

Figure 5. N_2 adsorption isotherms and corresponding pore size distributions of functionalized silica supports prepared without (A,B) and with RaMeβCD (C,D): (a) non-functionalized support; (b) support@CAG; (c) support@CAG@CALB.

This suggests that the distribution of grafted amino groups is most likely non-uniform, leading to pore blocking effects that result from the preferential reaction of these groups with the exposed surface of the small particles decorating the larger ones. Similar observations were made previously by Ritter *et al.* [55] that led to conclusion that the small pore diameters facilitate the pore blockage upon functionalization with APTMS due to the preferential location of amino groups at the pore entrances. However, in our bimodal material, we also noticed a broadening of the pore size distributions related to the largest mesopores, indicating that some silanes could also be located at the surface of particles [56]. A similar trend on the evolution of pore size distributions was observed upon lipase immobilization, suggesting higher grafting density of the protein at the outer surface of the carrier. On the other hand, the RaMeβCD-SiO_2@CAG support displayed a different behavior with regard to the binding of CALB, showing a progressive decrease in the pore diameter and pore volume indicative of the filling of pores with the functional groups and the protein (Figure 5 D, Table 1). Such changes are consistent with the higher pore accessibility of this material and its more uniform internal pore structure, in agreement also with TEM observations (Figure 3). Moreover, it is worth noting that the porosity and pore size distributions of our materials are measured under dried conditions, which usually involve contraction of the pore space, thus underestimating the pore diameter of silica in water. Although the pore size cannot be fairly compared with the real dimensions of the enzyme, it is assumed that the hydrated surface of silica under immobilization conditions could further facilitate the diffusion of the protein through the silica framework due to the expansion of its pore structure in water.

Confocal laser scanning microscopy observations provided further evidence for the different spatial distribution of the enzyme within the two supports (Figure S11, ESI). Thus, a diffuse fluorescence of relatively high intensity, localized mainly on the particle surface, was obtained upon illuminating the FITC-labelled CALB immobilized on CD-free SiO_2. Several large asymmetric fluorescent spots were present all over the sample, which are probably derived from inter-protein interactions on the surface of the densely packed fractal aggregates. In contrast, RaMeβCD-SiO_2 displayed more homogeneous fluorescence signal and the bright luminescent spots observed in this sample were smaller and appeared more regular in size and shape, consistent with a higher degree of uniformity in the distribution of enzyme within the particles.

2.4 Catalytic activity. In our experiments, the oxidation of DFF to FDCA was assessed by adding 2.0 equivalents of aqueous H_2O_2 (30% *v/v*) in a mixture of ethyl acetate (EtOAc) and *tert*-butanol (tBuOH) (1:1 *v/v*) containing 10 mM DFF.

As expected from our characterization results, the overall activity of the immobilized lipase was dependent on the immobilization procedure and the type of support (Table 2). Indeed, while the free lipase was inactive after 7 hours of reaction at 40 °C (entry 1), the DFF conversion reached 87% when 2 mg CALB was grafted on the surface of SiO_2@CAG particles (entry 2). However, the FDCA yields were still low (29%), FFCA being the major product (58%). The specific activity achieved was 14.4 μmol g^{-1} min^{-1}, while the total turnover number (TTN) accumulated after 7 hours of reaction was 199 mol mol^{-1}, corresponding to a turnover frequency (TOF) of 0.475 min^{-1}. Interestingly, full conversion of DFF was achieved with the RaMeβCD-SiO_2@CAG@CALB biocatalyst under the same reaction conditions, which resulted in more than 2-fold increase in the FDCA yield (69%, entry 3). Similarly, the specific activity, TTN and TOF

were almost 2.4 times higher than those obtained with SiO_2@CAG@CALB. Nevertheless, upon increasing the reaction time to 24 hours, both biocatalysts gave total DFF conversion with quantitative FDCA yields (>99%), resulting in accumulated TTN higher than 660 (entries 4, 5). It is worth noting that the activities obtained with our catalysts were higher than those reported in previous research with the commercial Novozym 435 [57], where the maximum FDCA yield that could be obtained after 24 hours reaction was 88%, corresponding to a TTN of 293.

For comparison, the activity of CALB adsorbed on RaMeβCD-SiO_2@C or grafted on RaMeβCD-SiO_2@AG was also evaluated. Under identical reaction conditions, RaMeβCD-SiO_2@C@CALB was not active (entry 6), while a DFF conversion of 63% was achieved with RaMeβCD-SiO_2@AG@CALB without any formation of FDCA (entry 7). This result confirms that although the hydrophobic interactions with the trimethyl groups from CTMS are not strong enough to maintain the protein anchored to the support, the hydrophobic microenvironment that these groups create is crucial for the interfacial activation of the lipase [58]. Indeed, as shown by Manoel *et al.* [59] immobilization on hydrophobic surfaces implies the open form of the lipase. It is well known that CALB does not have a lid domain, but presents an interfacial hyperactivation upon contact with hydrophobic surfaces, exposing its active site towards the substrate [60]. On the basis of our previous findings [42], the CTMS/SiO_2 molar ratio was fixed at 0.3. Increasing or reducing the CTMS/SiO_2 ratios caused a decrease in the FDCA yield due to denaturation of lipases in highly hydrophobic surfaces and strong water-surface interactions on hydrophilic ones that tend to shield the protein, causing its desorption [61].

Table 2. Catalytic performance of immobilized lipase CALB in the oxidation of DFF to FDCA.[a]

Entry	Catalyst	Enzyme loading (mg)	Immobilization efficiency (%)[b]	DFF conversion (%)	Yield (%)		Specific activity (µmol g^{-1} min^{-1})[f]	TTN (mol mol^{-1})[g]	TOF (min^{-1})[h]
					FFCA (%)	FDCA (%)			
1	Free CALB-7h	-	-	0	0	0	0	0	0
2	SiO_2@CAG[c]@CALB[d]-7h	1.92	96	87	58	29	14.4	199.4	0.475
3	RaMeβCD-SiO_2@CAG@CALB-7h	1.98	99	100	31	69	33.2	460.0	1.095
4	SiO_2@CAG@CALB-24h[e]	1.92	96	100	<1	>99	>49.1	>680.6	>1.621
5	RaMeβCD-SiO_2@CAG@CALB-24h	1.98	99	100	<1	>99	>47.6	>660.6	>1.571
6	RaMeβCD-SiO_2@C@CALB-7h	1.38	69	0	0	0	0.0	0.0	0.000
7	RaMeβCD-SiO_2@AG@CALB-7h	1.74	87	63	63	0	0.0	0.0	0.000

[a]Reaction conditions: 10 mM DFF, 2 mL EtOAc/tBuOH (1:1, v/v), sequential addition of 2.0 equivalents aqueous H_2O_2 (30% v/v) every hour for seven hours, temperature 40 °C, reaction time 7 hours, [b]Calculated from Equation 3 (see experimental part ESI), [c]CTMS/SiO_2 molar ratio = 0.33, APTMS/SiO_2 molar ratio = 0.17 and GAH/APTMS molar ratio = 1.1, [d]2 mg CALB in 20 mg support (1.33 mg/mL CALB in the immobilization solution),[e]reaction time = 24 hours, [f]specific activity was calculated as µmol of product formed (two µmol peracid per µmol of FDCA) per g of protein in one minute, [g]TTN = moles of FDCA formed divided by moles of protein, [h]TOF = TTN divided by reaction time.

To evaluate the recyclability of the two biocatalysts, 10 mM DFF was incubated in the EtOAc/t-BuOH (1:1 v/v) mixture for oxidation at 40 °C for 24 hours for each reaction cycle. The immobilized lipase was collected by centrifugation after each cycle, rinsed three times with the EtOAc/tBuOH (1:1, v/v) mixture and subsequently dried under vacuum before being reused for the next reaction cycles.

As shown previously [62], the furanic compounds formed during this reaction are likely to create pH-gradients in the immediate vicinity of the lipase due to the carboxylic acid groups that they bear in their cycle, provoking a complete inhibition of the enzyme activity. Moreover, under acidic conditions, protein leakage could also occur due to the very favorable hydrolysis of the Schiff base. Indeed, after the first reaction cycle, the FTIR spectra indicated a reduction in the intensity of the imine vibration at 1640 cm^{-1} for the RaMeβCD-SiO_2@CAG@CALB catalyst and total disappearance of this band for the SiO_2@CAG@CALB one (Figure S12 ESI). However, although the levels of enzyme leakage were different, complete deactivation of the lipase occurred in both systems due to the drop of the pH below 3.0.

To circumvent those limitations, a shell of a pH-sensitive polymer, the poly(4-vinylpyridine) (P4VP), was deposited on the biocatalyst surface. P4VP has a pKa equal to 4.5 and can interact with the functional groups available on the protein surface through its pyridine units. When the pH of the reaction mixture decreases below 4.5, P4VP undergoes protonation, causing swelling of the polymer chain and a reduction of the pH-gradient created near the biocatalyst surface [63, 64]. Therefore, to some extent, the polymer shell acts as a solid buffer protecting the lipase from denaturation [65].

With 20 wt.% surface coverage of P4VP, the activities obtained with both biocatalysts across five consecutive runs are shown in Figure 6. Whilst SiO_2@CAG@CALB caused the DFF conversion to drop by approximately one half (52%), almost full conversion (>90%) was achieved with RaMeβCD-SiO_2@CAG@CALB, which exhibited also higher selectivity for the FDCA formation. Thus, the FDCA yield was almost quantitative (> 99%) in the first two cycles, but it decreased to 72% after the third cycle, FFCA being the only intermediate (28%). In the last two cycles, FDCA was present as approximately 39% of the reaction mixture, while the yield obtained with the SiO_2@CAG@CALB biocatalyst was twice lower (19%). The rapid decrease in the FDCA yield from the third cycle can be related to the loss of the smallest particles along successive rinsing steps that caused a decrease in the amount of enzyme remaining in the reaction mixture. Indeed, after the fifth cycle, we were able to recover only 30% of the initial amount of solid (6.4 mg *vs.* 20.2 mg). However, the rinsing solution was able to catalyze efficiently the DFF oxidation giving 100% conversion. This is an indication that the enzyme was held tightly on the surface of functionalized silica particles and was not released into the rinsing solution. Further work in this direction is still necessary to reduce losses of fine particles and improve the biocatalyst separation efficiency.

Taken together, our results indicate that incorporation of CALB within the pores of the RaMeβCD-templated matrix followed by subsequent deposition of a poly(4-vinylpyridine) shell appears as a promising tool to bypass problems associated with lipase degradation under acidic conditions. Moreover, owing to its peculiar physicochemical properties (Figure S6 ESI), the methylated cyclodextrin may also provide a benign surrounding microenvironment for the protein. Thus, its high degree of hydrophobicity may contribute to the interfacial activation of

CALB and its unique surface-active properties may be beneficial for reducing the steric constraints, maintaining the immobilized lipase in a flexible conformation [66, 67].

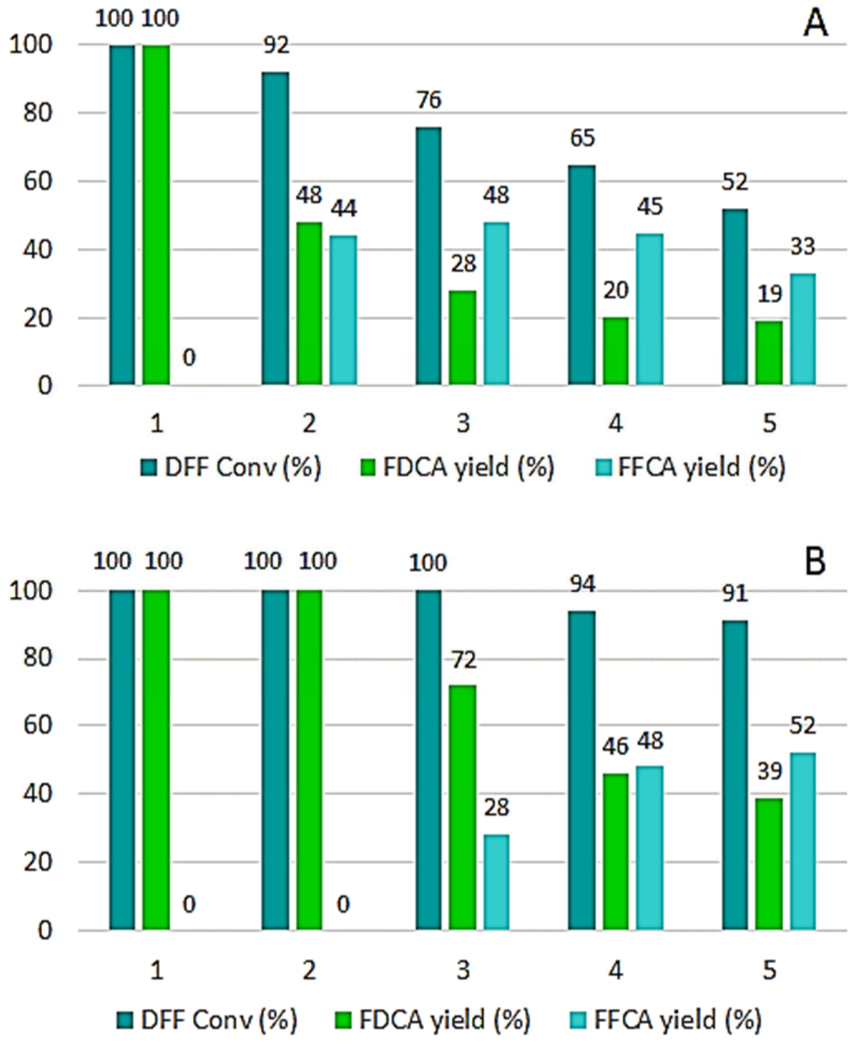

Figure 6. Catalytic recyclability of SiO_2@CAG@CALB@P4VP (A) and RaMeβCD-SiO_2@CAG@CALB@P4VP (B) biocatalysts. Reaction conditions: 10 mM DFF, 2 mL EtOAc/tBuOH (1:1 v/v), sequential addition of 2.0 eq. H_2O_2 (30% v/v) every hour for seven hours, temperature 40°C, reaction time 24 hours.

3. Conclusions

In summary, we have prepared and characterized two types of silica particles - one by conventional Stöber process in alkaline medium using the tetraethyl orthosilicate (TEOS) as silica source and the other by a modified Stöber process using the randomly methylated β-cyclodextrin (RaMeβCD) as structure directing agent. The first material consisted of 75-nm sized particles decorated on their surface with 6-nm sized nanoparticles and presented a bimodal pore size distribution with average pore diameters of 3.4 nm and 33 nm. Differently, the second material was composed of unimodal 8 nm-sized particles showing 11.2 nm-sized mesopores and a pore volume that was twice as high as that of the CD-free material (0.969 cm^3/g *vs.* 0.487 cm^3/g). In both syntheses, lipase B from *Candida antarctica* (CALB) was immobilized on the pre-functionalized supports by covalent bonding. Results revealed differences on the location of the enzyme, which was found either to anchor on the outer peripheral surface of CD-free particles or to be incorporated inside the pores of RaMeβCD-templated material. The catalytic activity of the immobilized biocatalysts was then evaluated in the oxidation of 2,5-diformylfuran (DFF) to 2,5-furandicarboxylic acid (FDCA). While the free enzyme was not active under the employed reaction conditions, interfacial activation was observed upon immobilizing lipase on the functionalized supports. Incorporation of CALB into the pores of RaMeβCD-templated material resulted in enhanced enzyme properties as compared to immobilization on surface. Thus, full DFF conversion was achieved after 7h at 40°C and the FDCA yields were two-fold higher with respect to the reference catalyst. Notably, CALB incorporated into the pores could be recycled five times, retaining more than 90% of its initial activity compared to 52% activity for the surface-bound lipase. This work can provide useful insights into the design of cyclodextrin-

based materials for efficient immobilization of other lipases and improvement of their functionality.

Acknowledgments

Chevreul Institute (FR 2638), Ministère de l'Enseignement Supérieur, de la Recherche et de l'Innovation and FEDER are acknowledged for supporting and funding this work. C.D. is grateful to the Région Hauts-de-France and the University of Artois who funded his PhD grant. We thank Dr E. Richard for access to Confocal Laser Scanning Microscope and technical advices, as well as the Research Federation FRABio (Univ. Lille, CNRS, FR 3688) for providing the scientific and technical environment conducive to achieving this work. We are grateful to D. Prevost, J. Ternel, A. Addad and L. Burylo for technical assistance with the reactor setup, NMR, TEM and SAXS respectively, as well as N. Kania for help with HPLC and TG analyses. The TEM facility in Lille is supported by the Conseil Regional des Hauts-de-France and the European Regional Development Fund (ERDF).

REFERENCES

[1] R. G. Burns, R. P. Dick (Eds), Enzymes in the Environment. Activity, Ecology, and Applications. New York, NY: Marcel Dekker Inc. (2002).

[2] J. A. Prescher, C. R. Bertozzi, Chemistry in living systems, Nature Chem. Biol. 1 (2005) 13-21.

[3] H. Yoshizumi, N. Matsumoto, O. Fukuda, O. Fukushi, Process for producing alcohol by fermentation without cooking, US Patent (1985) 4,514,496.

[4] H. Claus, K. Mojsov, Enzymes for wine fermentation: Current and perspective applications, Fermentation 4 (2018) 52.

[5] P.F. Fox, L. Stepaniak, Enzymes in cheese technology, Int. Dairy J. 3 (1993) 509-530.

[6] A. Kunamneni, S. Singh, Response surface optimization of enzymatic hydrolysis of maize starch for higher glucose production, Biochem. Eng. J. 27 (2005) 179-190.

[7] O. Kirk, T. V. Borchert, C. C. Fuglsang, Industrial enzyme applications, Curr. Opin. Biotechnol. 13 (2002) 345-351.

[8] J. B. van Beilen, Z. Li, Enzyme technology: an overview, Curr. Opin. Biotech. 13 (2002) 338-344.

[9] V. Tournier, C. M. Topham, A. Gilles, B. David, C. Folgoas, E. Moya-Leclair, E. Kamionka, M. L. Desrousseaux, H. Texier, S. Gavalda, M. Cot, E. Guémard, M. Dalibey, J. Nomme, G. Cioci, S. Barbe, M. Chateau, I. André, S. Duquesne, A. Marty, An engineered PET depolymerase to break down and recycle plastic bottles, Nature 580 (2020) 216-219.

[10] J.M. Thomas, R. Raja, Designing catalysts for clean technology, green chemistry, and sustainable development, Annu. Rev. Mater. Res. 35 (2005) 315-350.

[11] N. S. Scrutton, Enzymes make light work of hydrocarbon production, Science 357 (2017) 872-873.

[12] R. A. Sheldon, Enzyme immobilization: the quest for optimum performance, Adv. Synth. Catal. 349 (2007) 1289-1307.

[13] D. N. Tran, K. J. Balkus, Jr., Perspective of recent progress in immobilization of enzymes, ACS Catal. 1 (2011) 956-968.

[14] C. Garcia-Galan, A. Berenguer-Murcia, R. Fernandez-Lafuente, R. C. Rodrigues, Potential of different enzyme immobilization strategies to improve enzyme performance, Adv. Synth. Catal. 353 (2011) 2885-2904.

[15] U. Hanefeld, L. Gardossi, E. Magner, Understanding enzyme immobilization, Chem. Soc. Rev. 38 (2009) 453-468.

[16] K. Hernandez, R. Fernandez-Lafuente, Control of protein immobilization: Coupling immobilization and site-directed mutagenesis to improve biocatalyst or biosensor performance, Enzyme Microb. Tech. 48 (2011) 107-122.

[17] R. Fernandez-Lafuente, Stabilization of multimeric enzymes: Strategies to prevent subunit dissociation, Enzyme Microb. Tech. 45 (2009) 405-418.

[18] M. Li, S. Qiao, Y. Zheng, Y. H. Andaloussi, X. Li, Z. Zhang, A. Li, P. Cheng, S. Ma, Y. Chen, Fabricating Covalent Organic Framework Capsules with Commodious Microenvironment for Enzymes, J. Am. Chem. Soc. 142 (2020) 6675–6681.

[19] C. Mateo, J. M. Palomo, G. Fernandez-Lorente, J. M. Guisan, R. Fernandez-Lafuente, Improvement of enzyme activity, stability and selectivity via immobilization techniques, Enzyme Microb. Tech. 40 (2007) 1451-1463.

[20] F. Secundo, Conformational Changes of Enzymes Upon Immobilization. Chem. Soc. Rev. 42 (2013) 6250-6261.

[21] M. Hartmann, X. Kostrova, Immobilization of enzymes on porous silicas - benefits and challenges, Chem. Soc. Rev. 42 (2013) 6277-6289.

[22] L. Bayne, R. V. Ulijn, P. J. Halling, Effect of pore size on the performance of immobilized enzymes, Chem. Soc. Rev. 42 (2013) 9000-9010.

[23] Y. Xiao, M. Zheng, Z. Liu, J. Shi, F. Huang, X. Luo, Constructing a Continuous Flow Bioreactor Based on a Hierarchically Porous Cellulose Monolith for Ultrafast and Nonstop Enzymatic Esterification/Transesterification, ACS Sustainable Chem. Eng. 7 (2019) 2056-2063.

[24] J. Gao, W. Kong, L. Zhou, Y. He, L. Ma, Y. Wang, L. Yin, Y. Jiang, Monodisperse core-shell magnetic organosilica nanoflowers with radial wrinkle for lipase immobilization, Chem. Eng. J. 309 (2017) 70-79.

[25] Y. Du, J. Gao, L. Zhou, L. Ma, Y. He, Z. Huang, Y. Jiang, Enzyme nanocapsules armored by metal-organic frameworks: A novel approach for preparing nanobiocatalyst, Chem. Eng. J. 327 (2017) 119-1197.

[26] L. Huang, X. Yan, M. Kruk, Synthesis of ultralarge-pore FDU-12 silica with face-centered cubic structure, Langmuir 26 (2010) 14871-14878.

[27] J. Fan, C. Yu, J. Lei, Q. Zhang, T. Li, B. Tu, W. Zhou, D. Zhao, Low-temperature strategy to synthesize highly ordered mesoporous silicas with very large pores, J. Am. Chem. Soc. 127 (2005) 10794-10795.

[28] J. Szejtli, Introduction and general overview of cyclodextrin chemistry, Chem. Rev. 98 (1998) 1743-1753.

[29] R. Breslow, S. D. Dong, Biomimetic reactions catalyzed by cyclodextrins and their derivatives, Chem. Rev. 98 (1998) 1997-2011.

[30] R. Villalonga, R. Cao, A. Fragoso, Supramolecular Chemistry of Cyclodextrins in Enzyme Technology, Chem. Rev. 107 (2007) 3088-3116.

[31] C. David, M. C. Millot, E. Renard, B. J. Sebille, Coupling of antibodies to β-cyclodextrin-coated gold surfaces via an intermediate adamantyl-modified carboxymethylated dextran layer, J. Inclusion Phenom. Macrocycl. Chem. 44 (2002) 369-372.

[32] M. Holzinger, M. Singh, S. Cosnier, Biotin-β-Cyclodextrin: A New Host–Guest System for the Immobilization of Biomolecules, Langmuir 28 (2012) 12569-12574.

[33] S. Polarz, B. Smarsly, L. Bronstein, M. Antonietti, From cyclodextrin assemblies to porous materials by silica templating, Angew. Chem., Int. Ed. 40 (2001) 4417-4421.

[34] B. H. Han, M. Antonietti, Cyclodextrin-based pseudopolyrotaxanes as templates for the generation of porous silica materials, Chem. Mater. 14 (2002) 3477-3485.

[35] B. H. Han, B. Smarsly, C. Gruber, G. Wenz, Towards porous silica materials via nanocasting of stable pseudopolyrotaxanes from alpha-cyclodextrin and polyamines, Microporous Mesoporous Mater. 66 (2003) 127-132.

[36] R. Bleta, S. Menuel, B. Léger, A. Da Costa, E. Monflier, A. Ponchel, Evidence for the existence of crosslinked crystalline domains within cyclodextrin-based supramolecular hydrogels through sol-gel replication, RSC Adv. 4 (2014) 8200-8208.

[37] R. Bleta, C. Machut, B. Léger, E. Monflier, A. Ponchel, Coassembly of block copolymer and randomly methylated β-cyclodextrin: From swollen micelles to mesoporous alumina with tunable pore size, Macromolecules 46 (2013) 5672-5683.

[38] R. Bleta, A. Lannoy, C. Machut, E. Monflier, A. Ponchel, Understanding the role of cyclodextrins in the self-assembly, crystallinity, and porosity of titania nanostructures, Langmuir 30 (2014) 11812-11822.

[39] A. Lannoy, R. Bleta, C. Machut-Binkowski, A. Addad, E. Monflier, A. Ponchel, Cyclodextrin-directed synthesis of gold-modified TiO_2 materials and evaluation of their photocatalytic activity in the removal of a pesticide from water: Effect of porosity and particle size, ACS Sustainable Chem. Eng. 5 (2017) 3623-3630.

[40] R. Bleta, B. Schiavo, N. Corsaro, P. Costa, A. Giaconia, L. Interrante, E. Monflier, G. Pipitone, A. Ponchel, S. Sau, O. Scialdone, S. Tilloy, A. Galia, Robust mesoporous CoMo/γ-Al_2O_3 catalysts from cyclodextrin-based supramolecular assemblies for hydrothermal processing of microalgae: Effect of the preparation method, ACS Appl. Mater. Interfaces 10 (2018) 12562-12579.

[41] R. Bleta, S. Noel, A. Addad, A. Ponchel, E. Monflier, Mesoporous RuO_2/TiO_2 composites prepared by cyclodextrin-assisted colloidal self-assembly: towards efficient catalysts for the hydrogenation of methyl oleate, RSC Adv. 6 (2016) 14570-14579.

[42] C. Decarpigny, R. Bleta, A. Ponchel, E. Monflier, Confinement of Candida antarctica lipase B in a multifunctional cyclodextrin-derived silicified hydrogel and its application as enzymatic nanoreactors, ACS Applied Bio Mater. 2 (2019) 5568-5581.

[43] R. D. Schmid, R. Verger, Lipases: interfacial enzymes with attractive applications, Angew. Chem. Int. Ed. 37 (1998) 1608-1633.

[44] A. Basso, S. Serban, Industrial applications of immobilized enzymes - A review, Mol. Catal. 479 (2019) 110607.

[45] E. M. Anderson, K. M. Larsson, O. Kirk, One biocatalyst-Many applications: The use of Candida antarctica lipase B in organic synthesis, Biocatal. Biotransform. 16 (1998) 181-204.

[46] A. A. Tzialla, I. V. Pavlidis, M. P. Felicissimo, P. Rudolf, D. Gournis, H. Stamatis, Lipase immobilization on smectite nanoclays: characterization and application to the epoxidation of α-pinene, Bioresour Technol 101 (2010) 1587-1594.

[47] K. Hernandez, R. Fernandez-Lafuente, Lipase B from Candida antarctica immobilized on octadecyl Sepabeads: A very stable biocatalyst in the presence of hydrogen peroxide, Process Biochemistry 46 (2011) 873-878.

[48] R. A. Sheldon, Green and sustainable manufacture of chemicals from biomass: state of the art, Green Chem. 16 (2014) 950-963.

[49] X. Fei, J. Wang, J. Zhu, X. Wang, X. Liu, Biobased poly(ethylene 2,5-furancoate): No longer an alternative, but an irreplaceable polyester in the polymer industry, ACS Sustainable Chem. Eng. 8 (2020) 8471-8485.

[50] M. Krystof, M. Perez-Sanchez, P. Dominguez de Maria, Lipase-mediated selective oxidation of furfural and 5-hydroxymethylfurfural, Chem. Sus. Chem. 6 (2013) 826-830.

[51] P. Monsan, Optimization of glutaraldehyde activation of a support for enzyme immobilization. J. Mol. Catal. 3 (1978) 371-384.

[52] A. Ayral, J. Phallipou, T. Woignier, Skeletal density of silica aerogels determined by helium pycnometry, J. Mater. Sci. 27 (1992) 1166-1170.

[53] S. Kondo, H. Fujiwara, E. Okazaki, T. Ichii, The surface structure of ethoxylated silica gel, J. Coll. Interf. Sci. 75 (1980) 328-332.

[54] E. F. Vansant, P. Van Der Voort, K. C. Vrancken, Characterization and chemical modification of the silica surface. Vol. 93 Amsterdam, The Netherlands: Elsevier Science (1995).

[55] H. Ritter, D. Brühwiler, Accessibility of amino groups in postsynthetically modified mesoporous silica, J. Phys. Chem. C. 113 (2009) 10667-10674.

[56] M. J. Reber, D. Brühwiler, Mesoporous hybrid materials by simultaneous pseudomorphic transformation and functionalization of silica microspheres, Part. Part. Syst. Char. 32 (2015) 243-250.

[57] Y. Z. Qin, Y. M. Li, M. H. Zong, H. Wu, N. Li, Enzyme-catalyzed selective oxidation of 5-hydroxymethylfurfural (HMF) and separation of HMF and 2, 5-diformylfuran using deep eutectic solvents, Green Chem. 17 (2015) 3718-3722.

[58] C. José, M. V. Toledo, P. Nicolás, V. Lasalle, M. L. Ferreira, L. E. Briand, Influence of the nature of the support on the catalytic performance of CALB: experimental and theoretical evidence, Catal. Sci. Technol. 8 (2018) 3513-3526.

[59] E. A. Manoel, J. C. S. dos Santos, D. M. G. Freire, N. Rueda, Roberto Fernandez-Lafuente, Immobilization of lipases on hydrophobic supports involves the open form of the enzyme, Enzyme Microb. Technol. 71 (2015) 53-57.

[60] T. Zisis, P. L. Freddolino, P. Turunen, M. C. F. van Teeseling, A. E. Rowan, K. G. Blank, Interfacial activation of Candida antarctica lipase B: Combined evidence from experiment and simulation, Biochemistry 54 (2015) 5969-5979.

[61] I. Firkowska-Boden, X. Zhang, K. D. Jandt, Controlling protein adsorption through nanostructured polymeric surfaces, Adv. Healthcare Mater. 7 (2018) 1-19.

[62] A. Karich, S. B. Kleeberg, R. Ullrich, M. Hofrichter, Enzymatic preparation of 2,5-furandicarboxylic acid (FDCA)-A substitute of terephthalic acid by the joined action of three fungal enzymes, Microorganisms 6 (2018) 5.

[63] H. Wang, I. H. Lee, M. Yan, A general method to determine ionization constants of responsive polymer thin films, J. Coll. Interf. Sci. 365 (2012) 178-183.

[64] L. Nie, S. Liu, W. Shen, D. Chen, M. Jiang, One-pot synthesis of amphiphilic polymeric Janus particles and their self-assembly into supermicelles with a narrow size distribution, Angew. Chem., Int. Ed. 119 (2007) 6437-6440.

[65] J. J. Virgen-Ortiz, J. C. S. dos Santos, A. Berenguer-Murcia, O. Barbosa, R. C. Rodrigues, R. Fernandez-Lafuente, Polyethylenimine: a very useful ionic polymer in the design of immobilized enzyme biocatalysts, J. Mater. Chem. B 5 (2017) 7461-7490.[66] K. Griebenow, Y. D. Laureano, A. M. Santos, I. M. Clemente, L. Rodriguez, M. W. Vidal, G. Barletta, Improved enzyme activity and enantioselectivity in organic solvents by methyl-β-cyclodextrin, J. Am. Chem. Soc. 121 (1999) 8157-8163.[67] Y. Mine, K. Fukunaga, K. Itoh, M. Yoshimoto, K. Nakao, Y. Sugimura, Enhanced enzyme activity and enantioselectivity of lipases in organic solvents by crown ethers and cyclodextrins, J. Biosci. Bioeng. 95 (2003) 441-447.

Graphical abstract

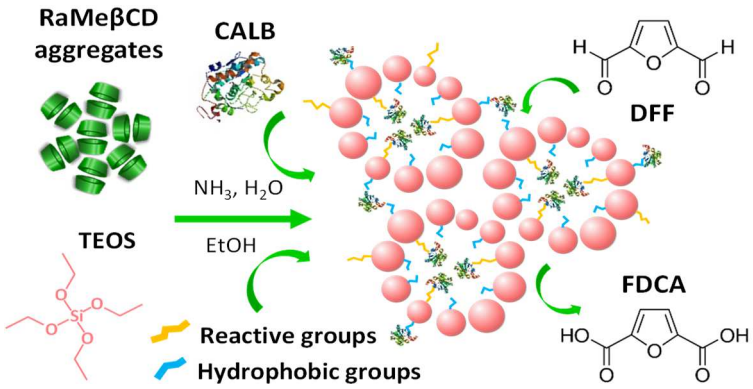

An enzymatic nanoreactor with enhanced catalytic performance was prepared by incorporating CALB within the pores of a methylated β-cyclodextrin-derived silica